Published in final edited form as:
Anal Chem. 2006 May 15; 78(10): 3406–3416. doi:10.1021/ac0600149.

Peak Capacity Optimization of Peptide Separations in Reversed-Phase Gradient Elution Chromatography:

Fixed Column Format

Xiaoli Wang, **Dwight R Stoll**, **Adam P Schellinger**, and **Peter W. Carr***
Department of Chemistry University of Minnesota 207 Pleasant Street SE Minneapolis, MN, 55455

Abstract

The optimization of peak capacity in gradient elution RPLC is essential for the separation of multi-component samples such as those encountered in proteomic research. In this work we study the effect of gradient time (t_G), flow rate (F), temperature (T) and final eluent strength (ϕ_{final}) on the peak capacity of separations of peptides that are representative of the range in peptides found in a tryptic digest. We find that there are very strong interactions between the individual variables (e.g. flow rate and gradient time) which make the optimization quite complicated. On a given column, one should first set the gradient time to the longest tolerable and then set the temperature to the highest achievable with the instrument. Next, the flow rate should be optimized using a reasonable but arbitrary value of ϕ_{final}. Last, the final eluent strength should be adjusted so that the last solute elutes as close as possible to the gradient time. We also develop an easily implemented, highly efficient and effective Monte Carlo search strategy to simultaneously optimize all the variables. We find that gradient steepness is an important parameter that influences peak capacity and an optimum range of gradient steepness exists in which the peak capacity is maximized.

INTRODUCTION

The last decade has witnessed a huge increase of interest in the analysis of complex biological mixtures.[1, 2] Currently, High-Performance Liquid Chromatography (HPLC) operated under gradient conditions is one of the premier bio-separation techniques due to its high efficiency and resolving power.[3] Specifically, reversed-phase gradient elution chromatography has found many important applications in one-[4-7] and two-dimensional[8-11] separations of proteins and peptides.

Peak capacity is the most common metric of separation power in gradient elution chromatography. For most HPLC systems, typical peak capacities obtainable in a one-dimensional separation of peptides range from 100 to 400.[12] Continuing the pioneering work of Jorgenson in ultra-high pressure HPLC,[13] Shen et al. reported a peak capacity of 1500 in a 2000-minute, one-dimensional separation using a 200 cm long capillary column packed with 3 μm particles operated at 20 KPsi backpressure.[14] However, even the highest peak capacities yet reported compare poorly to the number of components in many biological samples (e.g. > 200,000 in enzymatic digests of cell extracts).[15, 16] As a result, only a small fraction of the observed peaks contain a single analyte. In this context, the Davis-Giddings statistical model of overlap (SMO)[17] makes it clear that one must increase the peak capacity of the separation to decrease the degree of peak overlap.

*To whom correspondence should be addressed (carr@chem.umn.edu)

In 1967, Giddings[18] first defined the peak capacity concept and derived an expression for isocratic/isothermal chromatography:

$$n_c = 1 + \frac{N^{1/2}}{4} \ln (t_n / t_1) \quad (1)$$

where N is the plate number, t_1 and t_n are the retention times of the *first* and the *last* peak (not the dead time and some arbitrary upper limit), respectively. Horvath and Lipsky[19] extendedGiddings's work to temperature programmed GC and gradient elution LC. They gave the following expression for the corresponding peak capacity based on the assumption that all peaks have the same width:

$$n_c = \left(N^{1/2}/4\right) [(t_n/t_1) - 1] \quad (2)$$

For consistency in this work we have changed the notation used by Giddings and Horvath to that of Grushka. Grushka[20] showed that the increment in peak capacity during an infinitesimal time increment is given by:

$$dn_c = dt/4\sigma \quad (3)$$

where 4σ is the peak base width at time t. By simply integrating eq 3 assuming that σ increases linearly with time, as it does under isocratic/isothermal elution, Grushka reproduced eq 1:

$$n_c = 1 + \frac{N^{1/2}}{4} \ln (t_n / t_A) \quad (4)$$

However, Grushka chose to define t_A as the column dead time and tn as the retention time of the last peak. If we assume that the peak width in gradient elution is approximately independent of retention,[21] integration of eq 3 gives:

$$n_c = 1 + \frac{t_n - t_A}{W} \quad (5)$$

where W is the fixed peak width. By his use of t_A, not the time of the first peak as per Giddings, it is evident that Grushka modified the peak capacity concept although he did not comment on the difference between his equation and Giddings'.

Since the time in which a solute can elute under gradient conditions actually extends from t_0 to $t_0 + t_D + t_G$ (t_0 is the column dead time, t_D is the dwell time and t_G is the gradient time), Snyder,[22] in contrast to Giddings and Horvath, estimated the time window as t_G and thus approximated the maximum possible peak capacity as:

$$n_c = 1 + \frac{t_G}{W} \approx \frac{t_G}{W} \quad (6)$$

However, realizing that a real sample generally occupies only a fraction of the maximum possible time window (t_G), Snyder[22] returned to the use of a time window based on the first

real and last real peak as initially formulated by Giddings and Horvath and then went on to define what he termed a "sample peak capacity" (n_c**):

$$n_c^{**} = \left(t_{R,n} - t_{R,1}\right)/W \tag{7}$$

where $t_{R,n}$ and $t_{R,1}$ are the same as t_n and t_1 in eqs 1 and 2, respectively. Clearly, t_G is the maximum possible time window that a real sample can occupy. Therefore, the peak capacity calculated from eq 6 is a *hypothetical maximum possible peak capacity*; it is always larger than the peak capacity calculated from eq 7. In this work we will compute the peak capacity using the same conceptual framework as was originally done by Giddings and Horvath and by Snyder in eq 7 but will drop Snyder's terminology, i.e. the "sample peak capacity" as this introduces a second name for a pre-existing concept. Thus we base our peak capacity on the first real peak (located at $t_{R,1}$).

Theories of gradient elution chromatography are well developed.[21, 23-25] Specifically, gradient theory based on Linear Solvent Strength Theory (LSST) provides a straightforward and accurate method for the prediction of both retention and peak width, and thus peak capacity, for small molecules as well as proteins and peptides.[26, 27] Based on this model, Stadalius et al. studied the effect of gradient time and column length on peak capacity calculated from eq 6.[28] In a completely theoretical work, Neue and Mazzeo[29] developed a detailed theory that relates peak capacity via eq 6 to the operational variables of gradient elution. They studied the influence of flow rate, gradient time and temperature on peak capacity mainly for small molecules and concluded that increasing the temperature of the column will improve the speed of the separation by reducing solvent viscosity and increasing solute diffusion. This is precisely in the same spirit as the pioneering theoretical studies of Antia and Horvath,[30] and Chen and Horvath[31] on the effect of temperature on speed in isocratic HPLC, which is confirmed in recent work from this laboratory.[32, 33]

Recently, Gilar et al. investigated the effect of the operational variables (e.g. flow rate and gradient time) and column format (e.g. column length and particle size) on the peak capacity via eq 6 of reversed-phase gradient elution separations of peptides.[12] It is very important to note that as the separation conditions (e.g. temperature, gradient steepness) are varied, both the peak width and the retention window will change, thus the peak capacity via eq 7 (n_c**) is the most important separation metric to be optimized for a *real* sample. In addition, optimization of the worst resolved pair of peaks is usually not of interest in the separation of complex samples with numerous severely overlapped peaks. Instead, optimizing the average resolution (R_{avg}) for all peak pairs is much more important. The experimental average resolution for a mixture of n components is defined by:

$$R_{avg} = \sum_{i=1}^{n-1} R_{i,i+1}/(n-1) \tag{8}$$

By inserting the fundamental definition of resolution for a given pair of solute *i* and *i+1* into eq 8 (t_R and W are the retention time and baseline peak width):

$$R_{i,i+1} = \frac{2\left(t_{R,i+1} - t_{R,i}\right)}{W_i + W_{i+1}} \tag{9}$$

and assuming a constant peak width of W_{avg} under gradient conditions, we can show that:

$$R_{avg}=\sum_{i=1}^{n-1}\left(\frac{t_{R,i+1}-t_{R,i}}{W_{avg}}\right)/(n-1)=\left(\frac{t_{R,n}-t_{R,1}}{W_{avg}}\right)/(n-1) \tag{10}$$

By comparing eq 10 with eqs 6 and 7, it is clear that the average resolution is proportional to the peak capacity computed via eq 7:

$$R_{avg}=n_c^{**}/(n-1) \tag{11}$$

Thus, optimizing the peak capacity (n_c**) is equivalent to optimizing the average resolution. In this paper, we first study the effect of the individual operational variables (gradient time, flow rate, temperature and final eluent strength) on the peak capacity (n_c**) of peptides for a fixed column format (i.e. fixed column length and particle diameter). We then use a Monte Carlo strategy to explore the multidimensional optimization and verify the conclusions reached by changing one variable at a time.

THEORY AND COMPUTATIONAL METHODS

Prediction of Retention Times

We used the Linear Solvent Strength Theory (LSST) of gradient elution to predict gradient retention times at a given temperature. The isocratic retention of a solute (ln *k*') is assumed to be a linear function of the volume fraction of the organic modifier (ϕ):

$$\ln\ k'=\ln\ k'_w - S\cdot\phi \tag{12}$$

where *S* is the slope of *ln k'* versus ϕ and *ln k'*$_w$ is the extrapolated solute retention in pure water. Using LSST theory, the retention time (t_R) in linear gradient elution is given as:[24]

$$t_R=t_0+t_D+\frac{t_0}{b}\ln\left[b\left(k'_0-\frac{t_D}{t_0}\right)+1\right] \tag{13}$$

where t_0 is the column dead time, t_D is the system dwell time, k'_0 is the isocratic retention factor in the initial eluent of the gradient. The gradient steepness (*b*) is defined as:

$$b=\frac{S\left(\phi_{final}-\phi_{initial}\right)V_m}{F\cdot t_G} \tag{14}$$

where *F* is the flow rate (mL/min), and t_G is the gradient time, V_m is the column dead volume (mL) and $\phi_{initial}$ and ϕ_{final} are the initial and final eluent compositions of the gradient, respectively.

To enable prediction of retention times under the various conditions, we collected data from three gradient "training" runs to obtain three experimental retention times for each solute ($t_{1,exp}$, $t_{2,exp}$, $t_{3,exp}$); we varied only the gradient time (t_G = 20, 40, 60 min) while keeping all other separation conditions (*T*, *F*, $\phi_{initial}$, ϕ_{final}) constant. In principle only two runs are necessary but more reliable results as well as an estimate of uncertainty can be obtained with three runs. Next, we used Microsoft Excel® to obtain the ln *k'*$_w$ and *S* values for each analyte.

The Solver add-in of Excel was used to find the ln k'_w and S that gave the best agreement between the predicted and experimental retention times at the three gradient times. After performing gradient training runs at three different temperatures (T = 40, 60, 80 °C), we fit the values of ln k'_w and S for each analyte against T^{-1} using simple functions (see discussion). Using these fits, the ln k'_w and S values of each analyte can be used to predict gradient retention times at different temperatures, gradient times, etc. Again, only two temperatures are needed but three were used to enhance the reliability of the predictions.

Prediction of Gradient Peak Width

The column's contribution to peak width at half height ($W_{1/2}$) was calculated using the following equation given by Snyder:[21]

$$W_{1/2}=\frac{2.35Gt_0\left(1+k'_f\right)}{\sqrt{N}} \tag{15}$$

where N is the *isocratic* plate number and G is the gradient band compression factor; k'_f is the solute retention factor when the solute is at the column exit and is given by:

$$k'_f=\frac{k'_0}{b\left[k'_0-(t_D/t_0)\right]+1} \tag{16}$$

Changes in column efficiency (N) as a function of flow rate were accounted by using the van Deemter equation. The coefficients of the van Deemter equation (A, B, C) were determined from an experimental flow curve obtained for the column used in this study.

The observed peak width not only includes peak broadening in the column, but also from the injector, connecting tubing, and the detector. Peak broadening upstream of the column under gradient conditions is usually negligible given that the solute is well retained in the initial eluent.[34] Therefore, we only considered the contribution from the post-column tubing ($\sigma^2_{t,\mathrm{pc}}$), the finite detector flow cell volume (σ^2_d) and the detector time constant (σ^2_τ):

$$\sigma^2_{total}=\sigma^2_{column}+\sigma^2_{extra}=\sigma^2_{column}+\left(\sigma^2_{t,\mathrm{pc}}+\sigma^2_d+\sigma^2_\tau\right) \tag{17}$$

The variance from dispersion in the tubing between the column and the detector was estimated by the Atwood-Golay method,[35] which corrects the Aris-Taylor equation to make it applicable for very short straight tubes. The variances from the detector flow cell volume and detector time constant were calculated using equations described by Sternberg.[36]

Temperature-Dependent Variables

Temperature plays an important role in the optimization of both isocratic[32] and gradient[37-39] separations. To predict separation parameters such as efficiency and backpressure as a function of the column temperature, we need to know how temperature affects the solvent viscosity and solute diffusion within the column. Chen and Horvath's empirical equation was used to calculate the viscosity as a function of temperature and eluent composition.[31] The solute diffusion coefficient was calculated as a function of temperature and eluent composition using the Wilke-Chang correlation.[40] The system backpressure (bar)

was estimated using Darcy's law and the Kozeny-Carman equation for the specific column permeability.[41]

Monte Carlo Multivariate Optimization Strategy

To fully search the multidimensional space of all variables affecting the gradient separation in a reasonable period of time, we used a Monte Carlo type optimization strategy. Specifically, we *simultaneously* optimized the four operational variables (F, T, t_G and ϕ_{final}) for a given column. First, a uniform random number generator was used to generate 5000 random values for each of the four variables within specified ranges. Each random number was rounded up to the nearest two decimal places for F, ϕ_{final} and the nearest one decimal place for T and t_G. For each condition, the corresponding gradient separation was characterized by calculating: the system backpressure (ΔP), each analyte's retention time (t_R) and peak width ($W_{1/2}$), the gradient steepness (b), and peak capacity (n_c**). We eliminated conditions requiring backpressures larger than 380 bar and conditions where the most retained analyte eluted after time t_G. The remaining acceptable conditions were then sorted according to their peak capacities to locate the optimum conditions.

EXPERIMENTAL SECTION

Materials and Reagents

All solutes were of reagent grade or better and were used without further purification. Eleven peptides (Gly-Phe, Neurotensin fragment 1-8, Phe-Phe, LHRH, Angiotensin II, [Val^5]-Antiogensin I, Substance P, Renin substrate, Momany peptide, Insulin chain B oxidized and Melittin) and Bovine Serum Albumin (BSA) were obtained from Sigma (St. Louis, MO, USA). Trifluoroacetic acid (TFA), 99%, was purchased from Aldrich (Milwaukee, WI, USA). The sample preparation procedures of the peptides were described elsewhere.[42]

HPLC water was obtained from a Barnsted Nanopure deionizing system (Dubuque, IA, USA) with an "organic-free" cartridge and a 0.2 μm filter. HPLC grade acetonitrile (ACN) was purchased from Sigma-Aldrich (Milwaukee, WI, USA). All pure solvents were filtered through a 0.45 μm nylon filtration apparatus (Lida Manufacturing Inc., Kenosha, WI) before use. All eluent mixtures were prepared gravimetrically and were not degassed prior to use.

HPLC Instrumentation and Columns

Chromatographic experiments were conducted using either an HP 1090 or an HP 1100 controlled by version A.10.01 Chemstation software (Agilent Technologies, Palo Alto, CA). The HP 1090 was equipped with a standard low-pressure mixing chamber, autosampler, photodiode-array UV detector, binary pump and a 1.7 μL micro-flow cell with a 6 mm path length. Column temperature was controlled using an eluent pre-heater and a column heating jacket that were generous gifts from Systec Inc. (New Brighton, MN). The HP1090 block heater was by-passed by directly connecting the injection valve to the Systec eluent pre-heater with a 10 cm length of PEEK tubing (0.007" i.d.) to reduce the system dwell volume. The eluent exiting the HPLC column was cooled before entering the detector using the built-in heat exchanger on the HP 1090. The HP 1100 was equipped with a low pressure mixing chamber, autosampler, quaternary pump, block heater, variable wavelength UV detector and a 13 μL flow cell with 10 mm path length. The dwell volumes were measured to be 0.30 mL and 0.90 mL on the HP 1090 and 1100 respectively.[43] All experiments were performed on a 50 mm × 2.1 mm i.d. Zorbax SB-C18 column containing 3.5 μm particles (80 Å pore diameter, gift from Agilent Technologies).

In calculating the variances due to extra-column broadening, we assumed a 38 cm long 0.007" tubing between the column exit and the detector (based on experimental measurement of the

HP 1090 heat exchanger). The detector flow cell volume was 1.7 μL and a detector time constant of 0.04 sec was used in the calculation.

Chromatographic Conditions

The gradient "training" runs to obtain the ln k'_w and S values of the eleven peptides were carried out on the HP 1090 system at a flow rate of 1.00 mL/min. Solvent A was 0.1% TFA (v/v) in H_2O and solvent B was 0.1% TFA (v/v) in 50:50 ACN:H_2O. The %B increased from 10% to 85% during the gradient. The separations of BSA tryptic peptides in Figure 12 were carried out on the HP 1100 system at either room temperature or 70 °C. The same solvent A was used but solvent B was 0.1% TFA (v/v) in 80:20 ACN:H_2O. At room temperature, the flow rate was set at 0.20 mL/min with a gradient of 6-74-100-100-6-6% B at 0-18-18.01-24-24.01-30 min. At 70 °C, the flow rate was set at 0.40 mL/min with a gradient of 6-35-100-100-6-6% B at 0-60-60.01-64-64.01-68 min. The detection was set at 214 nm and the injection volume was 5 μL.

RESULTS AND DISCUSSION

The eleven peptides used here were carefully chosen to span a range in retention time equivalent to that of the tryptic peptides from bovine serum albumin (BSA). We have shown that under a great variety of experimental conditions, this peptide mixture provides a retention window as well as peak widths and thus an experimental peak capacity very similar to those obtained with the very complex set of peptides in a BSA tryptic digest.[42] We thus believe that the results obtained here are quite applicable to a typical tryptic digest peptide mixture.

ln k'_w and S of the Eleven Peptides

To predict the retentions and peak widths of the eleven peptides at different temperatures, the ln k'_w and S values were plotted against $10^3/T$ (see Figure 1). First, the range of the S values is very large (10 – 60); this indicates that the retention of some peptides will be extremely sensitive to changes in eluent composition. The average value of S is approximately 40 and was used to calculate the average gradient steepness. Second, the ln k'_w increases approximately linearly with 1/T, as expected.[39, 44] Finally, the changes in the S values with temperature are relatively small and do not show any general trend. This is consistent with the findings of Snyder and coworkers.[45] The ln k'_w values were fitted against $10^3/T$ using a simple Padè polynomial: $y = A + [B \cdot x / (1 + C \cdot x)]$ to improve the quality of interpolation and S values were fitted against $10^3/T$ using a quadratic function: $y = A' + B' \cdot x + C' \cdot x^2$. The peak width averaged over all the peptides was used to calculate the peak capacity.

Effect of Gradient Time

The effect of gradient time (t_G) on peak capacity at different flow rates at fixed T, $\phi_{initial}$ and ϕ_{final} is shown in Figure 2A. In general, longer gradient times produce higher peak capacities although peak capacity tends to reach a limit at longer gradient times. This is consistent with previous studies[12] and the common belief that long gradients are needed to obtain high peak capacities. However, the rate of increase in peak capacity against gradient time is much greater at lower flow rates. Overall, the best peak capacities are found at intermediate flow rates (e.g. 0.40 mL/min) with a gradient time of 120 min. Clearly there is a strong interaction between flow rate and gradient time.

Since the peak capacity is determined by the ratio of the retention window ($\Delta t_R = t_{R,n} - t_{R,1}$) to the peak width ($W_{1/2}$), we looked at the effect of t_G on these parameters individually at 0.40 mL/min; these are presented in Figure 2B as plots of the values normalized to that at t_G = 10 min. Clearly as t_G increases the retention of the last peptide ($t_{R,n}$) increases to a much greater extent compared to the first peptide ($t_{R,1}$); this contributes to the approximately linear

increase in the retention window. On the other hand, the average peak width also increases with t_G, but to a much smaller relative extent. Overall, longer (shallower) gradients give higher peak capacities.

Effect of Flow Rate

In this section, we more thoroughly looked at the effect of flow rate on peak capacity to better understand why the peak capacity maximizes at 0.40 mL/min (see Figure 2A). First, we calculated the peak capacity as a function of flow rate at several different gradient times (see Figure 3A). One common behavior of all of these curves is that the peak capacity maximizes at intermediate flow rates. To help explain this trend, we also calculated the effect of flow rate on the retention windows and peak widths at t_G = 30 min (see Figure 3B). Evidently the retention window does not vary much with flow rate thus it does not contribute greatly to the trends in Figure 3A. However, the peak width varies quite a bit with flow rate and the narrowest peaks, on average, are obtained around 0.50 mL/min. This variation in peak width resembles a typical HETP versus flow rate. The optimum isocratic HETP for the 2.1 mm i.d. column used in this study is at a flow of 0.40 mL/min at 40 °C (data not shown). With t_G = 15 min, the best peak capacity occurs at 0.90 mL/min. However, with t_G = 120 min, the best peak capacity occurs at 0.30 mL/min. Therefore, we conclude that variations in efficiency with flow rate are by no means the only cause of the optimum peak capacity vs. flow rate. The optimum flow rate varies substantially with gradient time when the other factors (T and ϕ_{final}) are held constant. This is a very important observation. It says that one should not attempt to reach the highest peak capacity simply by using a flow rate which minimizes the isocratic HETP.

We also studied the effect of flow rate on peak capacity as a function of temperature at t_G = 30 min (see Figure 4A). In general, peak capacity increases with temperature; the increase is greater the higher is the flow rate. In addition, the optimum flow rate increases with temperatures (e.g. 0.50 mL/min at 40 °C and 0.80 mL/min at 100 °C). This can be rationalized, at least in part, by the fact that the flow rate that gives the minimum HETP in isocratic chromatography is higher at elevated temperatures.[46] Finally, this shows that at constant t_G, the effect of flow rate on the isocratic efficiency is the dominant factor that controls the gradient peak width, and thus the peak capacity.

Effect of Temperature

(1) Effect of Only Temperature—Figure 4B shows the effect of temperature on the peak capacity at low and high flow rates for t_G = 30 min. There are two patterns in this plot: at 2.00 mL/min, an increase in temperature always increases the peak capacity; in contradistinction, at 0.50 mL/min, an increase in temperature from low to intermediate values increases the peak capacity but then higher temperatures decrease the peak capacity.

To understand this complicated behavior, we studied the effect of temperature on the retention window and peak width separately (see Figure 5A and 5B). At both flow rates shown, the retention window decreases as the temperature is raised. The decrease in the retention window with temperature can be explained by the fact that the more retained solutes are generally more temperature sensitive than less retained solutes.[39] The peak width decreases due to faster diffusion of the peptides. At the lower flow rate (0.50 mL/min in Figure 5A), the peak width decreases faster than does the retention window from low to intermediate temperatures. Consequently, the peak capacity increases. In contrast, from intermediate to high temperatures, the retention window decreases faster than does the peak width thus peak capacity decreases. However, at 2.00 mL/min (Figure 5B), the peak width always decreases faster with temperature than does the retention window over the whole temperature range. Consequently, at high flow rate the peak capacity increases monotonically with temperature. This differential behavior at low and high flow rates is primarily due to the difference in the increase of isocratic efficiency

from 40 to 120 °C. At lower flow rates the less temperature dependent A term of the van Deemter equation is more important whereas at higher flow rates the very temperature dependent C term is more significant.[46]

(2) Effect of Temperature at Optimized ϕ_{final} but Fixed Flow Rate—As shown above the increase in peak capacity due to the decrease in peak width as the temperature is increased is opposed by the concomitant decrease in the retention window. We can easily compensate for the temperature induced decrease in retention window by decreasing the ϕ_{final} to maintain the retention range and thereby regain peak capacity. To demonstrate the feasibility of this approach, we used the Solver function of Excel to optimize the ϕ_{final} of the gradient to maximize the peak capacity at each temperature. The optimization was constrained such that the last peptide had to elute before the time t_G. Not surprisingly, the ϕ_{final} returned by Solver is always the value that makes the retention time of the last solute equal to t_G. A plot of peak capacity against temperature at the optimized ϕ_{final} is shown in Figure 6 (case b) along with the plot that results when the ϕ_{final} was fixed (case a). Clearly, this approach increases the peak capacity by moving the first and last eluting solutes further apart; however, at very high temperatures peak capacity still decreases.

(3) Effect of Temperature at Optimized ϕ_{final} and Flow Rate—In addition to the ϕ_{final}, the flow rate should also be adjusted as the temperature is changed to reach a global optimum peak capacity. Since the optimum flow rate that maximizes the isocratic efficiency increases with temperature (see Figure 4A), a fixed initial flow rate will gradually become sub-optimal as the temperature is raised. To compensate for this effect, we used Solver to *simultaneously* vary the ϕ_{final} and flow rate to maximize the peak capacity. The results are shown in Figure 6 (case c); the peak capacity now monotonically increases as the temperature is raised.

Figure 7A and 7B show the effect of temperature on the retention window and peak width for the three distinct conditions described above; these results confirm that adjusting the ϕ_{final} can compensate for the decrease in retention at higher temperatures. In addition, when only the ϕ_{final} is optimized (case b), the peak width actually increases at intermediate to high temperatures, presumably due to the reduced gradient steepness (caused by the smaller ϕ_{final}). Only when one simultaneously optimizes both the flow rate and ϕ_{final}, does the peak width decrease monotonically with temperature.

Effect of the Final Eluent Composition

The effect of the ϕ_{final} on peak capacity, when all other variables are kept constant, is shown in Figure 8A. Under these conditions, 40% ACN is the lowest ϕ_{final} that makes the last peptide elute before t_G. Further increases in the ϕ_{final} decrease the peak capacity. Figure 8B shows the effect of the ϕ_{final} on the retention window and peak width. As it is increased, both the retention window and peak width decrease; the decrease of the peak width is primarily due to the increase in gradient steepness and consequent decrease in k'_f. However, the retention window decreases more (> 60%) than the peak width (< 50%) and this causes an overall decrease in peak capacity. Clearly, given the otherwise fixed conditions, one ought to adjust the ϕ_{final} so that the last eluting solute is as close as possible to t_G. This agrees very well with the results shown in the discussion of temperature effects.

Recommended Peak Capacity Optimization Procedure

Because all of the work done above pertains to a set of peptides which do a good job of emulating the tryptic digest of BSA we believe that the optimization scheme suggested below should be useful for such mixtures. The results above clearly suggest that peak capacities increase monotonically with longer gradient times and higher temperatures provided that the

flow rate and ϕ_{final} are also optimized. At a fixed t_G and T, the peak capacity always maximizes at an intermediate flow rate (see Figure 3A and 4A). To check if the optimum flow rate depends on ϕ_{final}, we used Solver to find the optimum flow rate at three different values of ϕ_{final} at t_G = 60 min and T = 80 °C (see Table 1). It is evident that ϕ_{final} has only a small effect on the optimum flow rate. Therefore, we recommend the following peak capacity optimization procedure:

1. Set the gradient time to the longest tolerable value and set the temperature to the highest possible on the instrument
2. Optimize flow rate at any arbitrary but reasonable ϕ_{final}
3. At the optimized flow rate, adjust the ϕ_{final} so that the last solute elutes at t_G

Table 2 lists the optimum values of the flow rate and ϕ_{final} at various representative combinations of t_G and T. It is clear that the optimum values of flow rate and ϕ_{final} are quite different under the different conditions. In general, higher temperatures favor higher flow rates and lower ϕ_{final} while longer gradient times favor lower flow rates and lower ϕ_{final}. This is consistent with our results above.

Generalized Multivariate Optimization of Peak Capacity

It is evident from the results above that the individual variables interact very strongly during optimization (e.g. see the strong interaction between flow rate and temperature in Figure 4B). Thus it might appear that the recommended stepwise optimization procedure outlined above is simplistic. In this section we show by means of a simultaneous multidimensional Monte Carlo search that the procedure finds the optimum conditions.

(1) Robustness and Effectiveness of Monte Carlo Optimization—We generated 5000 sets of conditions using a random number generator with judiciously chosen ranges of the four key variables (F, t_G, T and ϕ_{final}) which influence peak capacity. The $\phi_{initial}$ was kept constant at 0.05 to maintain reasonable retention of the early eluting peptides. The separation quality (i.e. peak capacity) under each condition was then predicted. Conditions with pressures exceeding 380 bar (ΔP_{max} = 400 bar) or in which the last peptide is eluted after t_G were eliminated. We then sorted all remaining conditions (2651 conditions) to locate the optimum peak capacity. The best five conditions are listed in Table 3. It is clear that they all have long gradient times (57 – 60 min), high temperatures (69 – 77 °C), intermediate flow rates (0.39 – 0.53 mL/min) and low ϕ_{final} (0.38 – 0.41). This is fully consistent with our findings when we changed only one variable at a time. More importantly it is consistent with the optimization procedure described above. In general our results show that the highest optimized peak capacity is obtained with the largest value of t and at the highest temperature in agreement with Neue.[29] Although the optimum flow rate depends on both t_G and T once these are fixed the optimum flow rate is so slightly dependent on ϕ_{final} that it can be easily optimized in a univariate search. Finally the optimized peak capacity occurs when the last peak elutes just before t_G thus the last variable (ϕ_{final}) is so adjusted.

One prerequisite of the Monte Carlo search is that enough random conditions should be generated to avoid missing an optimum. If we assume a minimum resolution of 1 min for t_G, 0.02 mL/min for F, 1 °C for T and 0.01 for ϕ_{final}, more than 17 million conditions are needed to completely and uniformly cover the four-dimensional space. Consequently, we checked to see that the best conditions obtained from 5000 random search conditions were close to the global optimum. Therefore, at the very best condition found in the above search (condition 1 in Table 3), we deliberately changed one variable at a time while holding the other three variables at their original values. The effect of each variable on peak capacity is shown in Figure 9. It is evident that the gradient time and flow rate in condition 1 are exactly at their

optimum values. The temperature and ϕ_{final} deviate only slightly from their optimal values, but the changes in peak capacity are trivial. This verifies the robustness and effectiveness of the Monte Carlo search method.

(2) Effect of Gradient Steepness on Peak Capacity—The gradient steepness (b) is a very important parameter that changes as t_G, F and ϕ_{final} are varied (see eq 14). Therefore, we plotted the peak capacity against b for the 2651 conditions (see Figure 10). The contour of the data is mainly controlled by the range of gradient time at different gradient steepness. The range in t_G for conditions with large steepnesses (all have very short t_G) is small and thus their peak capacities do not vary much. On the other hand, the range in t_G for conditions with intermediate steepness is much larger since many different combinations of t_G and F can lead to similar b values (see eq 14); thus their peak capacities vary substantially. Further examination of Figure 10 suggests that the gradient steepness is a very important factor that influences peak capacity. First, it is clear that the use of very steep gradients (large b values resulting from low F or short t_G) is very detrimental to maximizing the peak capacity. Second, too low gradient steepnesses also cause reduced peak capacities even under conditions where all experimental variables are changed. In fact, very shallow gradient separations in the limit become the same as isocratic elution and it is common knowledge that isocratic elution is inferior to gradient elution in generating high peak capacities. Overall, peak capacity is maximized within an optimum range of b values between 0.02 and 0.07.

The existence of the optimum range of b is very important. First, it explains the behavior of peak capacity vs. t_G at different flow rates (see Figure 2A). At 0.10 mL/min, gradient steepness decreased from 1.6 at t_G = 10 min to 0.13 at t_G = 120 min. In this range of b, the peak capacity increased dramatically. However, at 2.00 mL/min, b varied from a near optimal value of 0.8 at t_G = 10 min to a sub-optimal value of 0.007 at t_G = 120 min. Therefore, the peak capacity increased only marginally. Second, it explains why the optimum flow rate at t_G = 15 min is higher than that at t_G = 120 min in Figure 3A: one needs a higher flow rate to reach the optimum gradient steepness range at the lower gradient times. We believe this is the major reason behind the difference between the flow rate that maximizes the peak capacity and the flow rate that optimizes the isocratic HETP (or N).

(3) Relationship between Peak Capacity and Average Resolution—As shown above, optimizing the peak capacity (n_c**) is, under the assumptions used, theoretically equivalent to optimizing the average resolution (see eq 11). We tested the accuracy of the theoretical relationship between average resolution and peak capacity. For each condition generated in the Monte Carlo search, we calculated the average resolution through eq 8 using the predicted retention times and peak widths of the eleven peptides. These average resolutions were then plotted against the peak capacities calculated via eq 7 (n_c**) and via eq 6 (n_c) as shown in Figure 11A and 11B, respectively. Clearly, the peak capacities via eq 7 correlate very well with the average resolutions and the slope of 9.82 agrees well with the theoretical value of 10 (n = 11). The slight deviation is mainly caused by the assumption in deriving eq 11 that all peaks have the same width; this is not exactly true. On the other hand, a very poor correlation between the peak capacities via eq 6 and the average resolution was observed (R^2 = 0.561). Since the average resolution has the most practical importance for optimizing the separation of complex samples, we justify the optimization of peak capacity via its definition by eq 7 and not eq 6.

Separation of BSA Tryptic Peptides at Non-optimal and Optimal Conditions

To demonstrate the utility of this work, we separated a peptide mixture from BSA tryptic digestion under a non-optimal condition and an optimal condition. As with the rest of this paper, the following discussion is focused on peak capacity, not peak capacity per unit time.

The non-optimal condition was adapted from a method used in a recently reported study.[47] Due to the different column i.d. and length, we adjusted the flow rate to maintain the same linear velocity and adjusted the gradient time to keep the same gradient steepness as used in their original work. The optimal separation condition was obtained by following the optimization procedure recommended here. We chose a gradient time of 60 min and a temperature of 70 °C since this is the highest temperature that the HP 1100 can give with good retention reproducibility. Subsequent Solver optimization returned a flow rate of 0.40 mL/min and a final eluent strength of 0.38 with a predicted peak capacity of 245.

The separations under the non-optimal and optimal conditions are shown in Figure 12A and 12B respectively. The peak capacity in Figure 12A was estimated to be 111 using the average peak width of the eleven peptides injected under the same conditions. It is evident that severe peak overlap exists for peptides eluted between 6 and 13 min; integration of the chromatogram indicated 75 peaks with signal to noise ratio higher than three. On the other hand, we estimated a peak capacity of 217 for the optimized separation in Figure 12B and 106 identified peaks suggesting a smaller degree of peak overlap. There are three observations worth discussion. First, we note that the peaks in Figure 12A are more than three times taller than those in 12B and this can be attributed to two major reasons: (1) peaks are narrower in 12A due to the steeper gradient (i.e. shorter t_G) and (2) peaks in 12A are more severely overlapped. Second, it should also be noted that the last eluting peptide in the BSA sample is less retained than that in the eleven peptides and this forced us to use a lower ϕ_{final} (0.30) compared to the ϕ_{final} (0.38) provided by the Solver solution. This decrease in ϕ_{final} caused a decrease in the gradient steepness which is mainly responsible for the lower observed peak capacity (217) compared to the predicted peak capacity (245). Finally, the use of higher temperature (i.e. 70 °C) in 12B caused many peptides to elute very close to the column dead time with poor resolutions. This problem might be solved by further decrease of the ϕ_{inital}.

CONCLUSIONS

We have studied the effect of the operational variables (F, t_G, T and ϕ_{final}) on the peak capacity of a set of peptides representative of a typical tryptic digest using a fixed column format under gradient elution RPLC conditions. The main conclusions are:

1. To maximize peak capacity, one should work at the longest tolerable gradient time and highest possible temperature achievable on the instrument. The flow rate should be optimized using any reasonable ϕ_{final}. Finally ϕ_{final} should be adjusted to make the last solute elute at t_G.
2. There are strong interactions between the individual operational variables. The optimal values of flow rate and ϕ_{final} depend strongly on the gradient time and temperature which is why they must be set first.
3. A Monte Carlo search strategy has been used to allow simultaneous multivariate optimization. The best condition was found to be very close to the global optimum and this verifies the robustness and effectiveness of the Monte Carlo approach.
4. Gradient steepness is an important parameter that influences peak capacity and an optimum range of gradient steepness (0.02 - 0.07) exists in which the peak capacity is maximized.
5. The peak capacity calculated via eq 7 is proportional to the measured average resolution while a poor correlation exists for the peak capacity as calculated from eq 6. Therefore, the peak capacity based on eq 7 is a more useful metric for the optimization of complex samples.

6. A simple mixture of eleven judiciously chosen peptides can do a good job of representing a typical tryptic digest.

ACKNOWLEDGEMENT

The numerous and insightful suggestions of Dr. Lloyd Snyder are gratefully acknowledged. The authors also acknowledge the financial support from the National Institute of Health (Grant # 5R01GM054585-09) and Agilent Technologies for the donation of the Zorbax SB-C18 column and Systec Inc. for the donation of the column heater.

GLOSSARY OF TERMS

n_c or n_c**, Peak capacity
t_R, Retention time (min)
W or $W_{1/2}$, Peak width at the base or at the half height (min)
R, Resolution
n, Number of components in the sample
F, Flow rate (mL/min)
T, Temperature (°C)
t_G, Gradient time (min)
$\phi_{initial}$ and ϕ_{final}, Initial and final eluent strength of the gradient
N, Isocratic plate count
k', Solute retention factor (isocratic)
k'_w, Extrapolated value of k' for $\phi = 0$
k'_0, Solute k' in initial eluent of the gradient
k'_f, Solute k' at the exit of the column defined by eq 16
S, Solute parameter defined by eq 12
b, Gradient steepness defined by eq 14
G, Gradient band compression factor
t_D, Gradient dwell time (min)
t_0, Column dead time (min)

REFERENCES

(1). Dunn WB, Ellis DI. Trends in Analytical Chemistry 2005;24:285–294.

(2). Issaq HJ. Electrophoresis 2001;22:3629–3638. [PubMed: 11699900]

(3). Neue UD. J. Chromatogr. A 2005;1079:153–161. [PubMed: 16038301]

(4). Jerkovich AD, Mellors JS, Jorgenson JW. LC-GC North America 2003;21:600–610.

(5). Shen Y, Moore RJ, Zhao R, Blonder J, Auberry DL, Masselon C, Pasa-Tolic L, Hixson KK, Auberry KJ, Smith RD. Anal. Chem 2003;75:3596–3605. [PubMed: 14570215]

(6). Shen Y, Zhao R, Belov ME, Conrads TP, Anderson GA, Tang K, Pasa-Tolic L, Veenstra TD, Lipton MS, Udseth HR, Smith RD. Anal. Chem 2001;73:1766–1775. [PubMed: 11338590]

(7). Shen Y, Zhao R, Berger S, Anderson GA, Rodriguez N, Smith RD. Anal. Chem 2002;74:4235–4249. [PubMed: 12199598]

(8). Bushey MM, Jorgenson JW. Anal. Chem 1990;62:161–167. [PubMed: 2310013]

(9). Chen J, Lee CS, Shen Y, Smith RD, Baehrecke EH. Electrophoresis 2002;23:3143–3148. [PubMed: 12298086]

(10). Stoll DR, Carr PW. J. Am. Chem. Soc 2005;127:5034–5035. [PubMed: 15810834]

(11). Wang H, Kachman MT, Schwartz DR, Cho KR, Lubman DM. Electrophoresis 2002;23:3168–3181. [PubMed: 12298089]

(12). Gilar M, Daly AE, Kele M, Neue UD, Gebler JC. J. Chromatogr. A 2004;1061:183–192. [PubMed: 15641361]

(13). MacNair JE, Lewis KC, Jorgenson JW. Anal. Chem 1997;69:983–989. [PubMed: 9075400]

(14). Shen Y, Zhang R, Moore RJ, Kim J, Metz TO, Hixson KK, Zhao R, Livesay ER, Udseth HR, Smith RD. Anal. Chem 2005;77:3090–3100. [PubMed: 15889897]
(15). Issaq HJ, Chan KC, Janini GM, Conrads TP, Veenstra TD. J. Chromatogr. B 2005;817:35–47.
(16). Wehr T. LCGC North America 2002;20:954–962.
(17). Davis JM, Giddings JC. Anal. Chem 1983;55:418–424.
(18). Giddings JC. Anal. Chem 1967;39:1027–1028.
(19). Horváth CG, Lipsky SR. Anal. Chem 1967;39:1893.
(20). Grushka E. Anal. Chem 1970;42:1142–1147.
(21). Snyder LR, Dolan JW. Advances in Chromatography 1998;38:115–187.
(22). Dolan JW, Snyder LR, Djordjevic NM, Hill DW, Waeghe TJ. J. Chromatogr. A 1999;857:1–20. [PubMed: 10536823]
(23). Jandera, P.; Churacek, J. Gradient elution in column liquid chromatography: theory and practice. Elsevier; Amsterdam: 1985.
(24). Schoenmakers PJ, Billiet HAH, Tijssen R, Galan LD. J. Chromatogr 1978;149:519–537.
(25). Snyder LR, Dolan JW, Gant JR. J. Chromatogr 1979;165:3–30.
(26). Stadalius MA, Gold HS, Snyder LR. J. Chromatogr 1984;296:31–59.
(27). Stadalius MA, Gold HS, Snyder LR. J. Chromatogr 1985;327:27–54.
(28). Stadalius MA, Quarry MA, Snyder LR. J. Chromatogr 1985;327:93–113.
(29). Neue UD, Mazzeo JR. J. Sep. Sci 2001;24:921–929.
(30). Antia FG, Horváth CG. J. Chromatogr 1988;435:1–15.
(31). Chen H, Horváth CG. Anal. Methods Instrum 1993;1:213–222.
(32). Thompson JD, Carr PW. Anal. Chem 2002;74:4150–4159. [PubMed: 12199587]
(33). Yang X, Ma L, Carr PW. J. Chromatogr. A 2005;1079:213–220. [PubMed: 16038307]
(34). Dolan JW. LCGC North America 2005;23:130–135.
(35). Atwood JG, Golay MJE. J. Chromatogr 1981;218:97–122.
(36). Sternberg JC. Advances in Chromatography 1966;2:205–270.
(37). Dolan JW, Snyder LR, Djordjevic NM, Hill DW, Saunders DL, Heukelem LV, Waeghe TJ. J. Chromatogr. A 1998;803:1–31. [PubMed: 9604325]
(38). Hancock WS, Chloupek RC, Kirkland JJ, Snyder LR. J. Chromatogr. A 1994;686:31–43. [PubMed: 7849982]
(39). Zhu PL, Snyder LR, Dolan JW, Djordjevic NM, Hill DW, Sander LC, Waeghe TJ. J. Chromatogr. A 1996;756:21–39. [PubMed: 9008855]
(40). Wilke CR, Chang P. Am. Inst. Chem. Eng. J 1955;1:264–270.
(41). Bird, RB.; Stewart, WE.; Lightfoot, EN. Transport Phenomena. John Wiley; New York: 1960.
(42). Wang X, Barber WE, Carr PW. J. Chromatogr. A 2006;1107:139–151. [PubMed: 16412451]
(43). Snyder, LR.; Glajch, JL.; Kirkland, JJ. Practical HPLC Method Development. Wiley-Interscience; New York: 1996.
(44). Melander W, Campbell DE, Horváth CG. J. Chromatogr 1978;158:215–225.
(45). Zhu PL, Dolan JW, Snyder LR. J. Chromatogr. A 1996;756:41–50.
(46). Yan B, Zhao J, Brown JS, Blackwell J, Carr PW. Anal. Chem 2000;72:1253–1262. [PubMed: 10740867]
(47). Qiu R, Regnier FE. Anal. Chem 2005;77:7225–7231. [PubMed: 16285669]

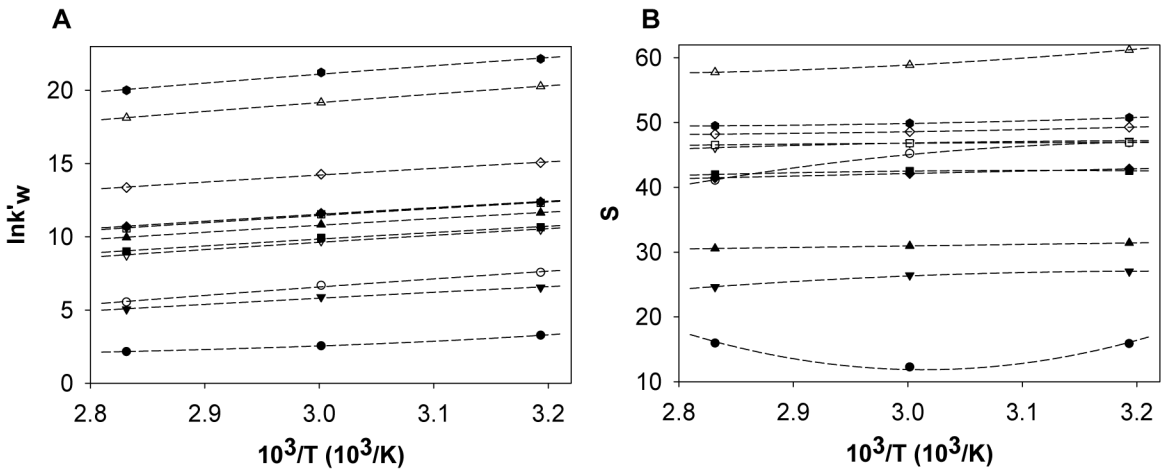

Figure 1.

Dependence of (A) ln k'_w values and (B) S values for eleven peptides on column temperature. The ln k'_w and S values were obtained from Solver using the retention time measured on a Zorbax SB-C18 column at three different gradient times at three temperatures. The dashed lines in (A) are fitted lines using a Padé equation and the dashed lines in (B) are fitted lines using a quadratic equation. Solutes: Gly-Phe (●); Neurotensin fragment 1-8 (○); Phe-Phe (▼); LHRH (▽); Angiotensin II (■); [Val^5]-Angiotensin I (□); Substance P (◆); Renin substrate (◇); Momany peptide (▲); Insulin chain B oxidized (△); Melittin (•).

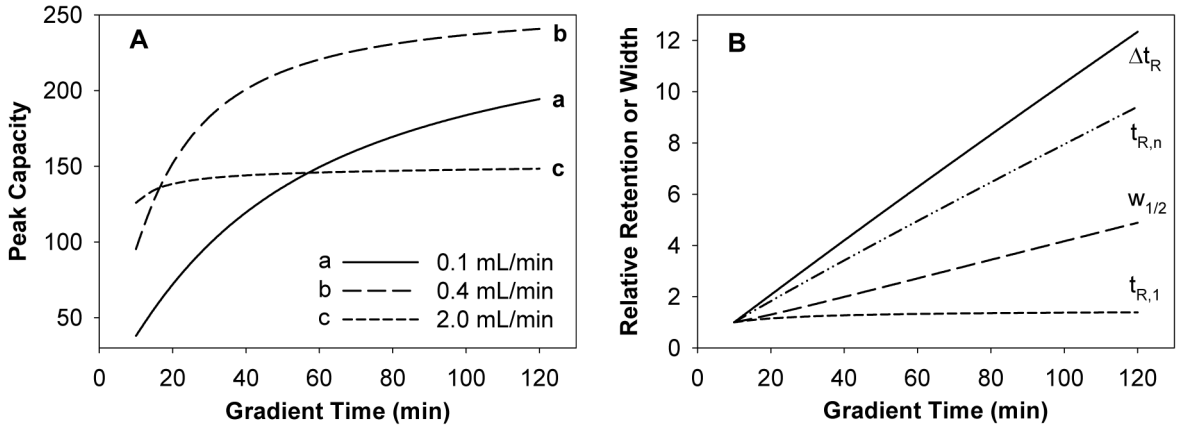

Figure 2.

(A) Effect of gradient time on peak capacity at various flow rates. (B) Effect of gradient time on relative retention window (Δt_R), average peak width at half height ($W_{1/2}$), retention time of first peptide ($t_{R,1}$) and last peptide ($t_{R,n}$) at 0.40 mL/min. The relative retention and peak width are normalized to their values at t_G = 10 min. Other variables: T = 40 °C, $\phi_{initial}$ = 0.05, ϕ_{final} = 0.50, V_D = 0.30 mL.

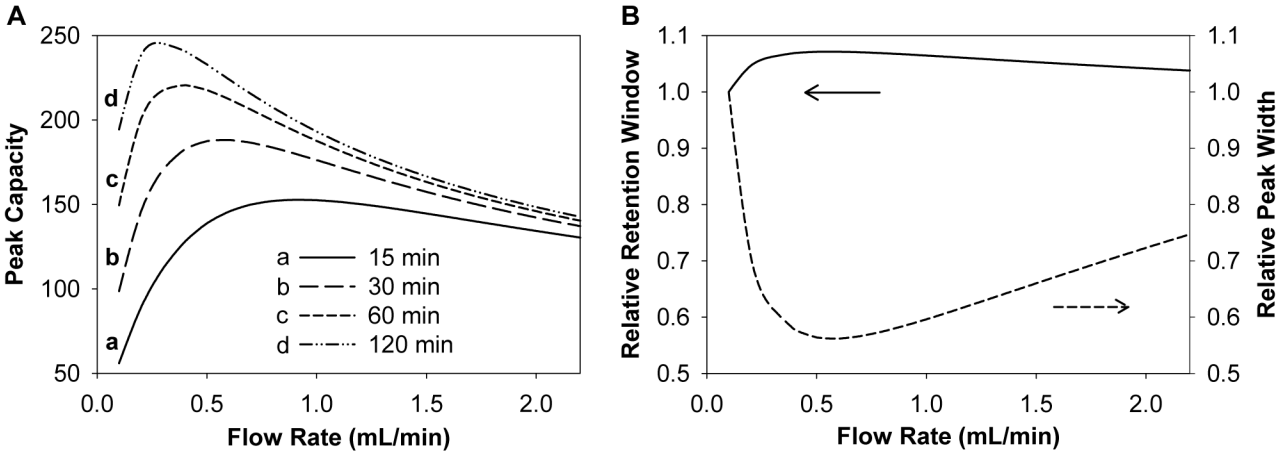

Figure 3.

Effect of flow rate on (A) peak capacity at various gradient times and (B) relative retention window and average peak width at half height in 30 min gradient. The relative retention window and average peak width are normalized to their values at F = 0.10 mL/min. Other variables: same as Figure 2.

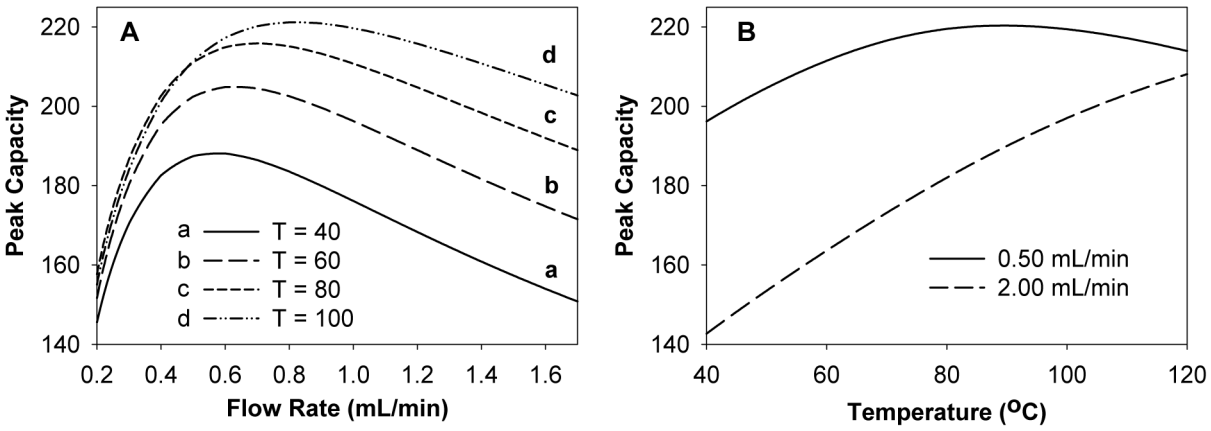

Figure 4.

Effect of flow rate and temperature on peak capacity. (A) Effect of flow rate at four temperatures. (B) Effect of temperature at two flow rates. Other variables: same as Figure 2 except t_G = 30 min. ϕ_{final} = 0.50 in (A) and ϕ_{final} = 0.43 in (B).

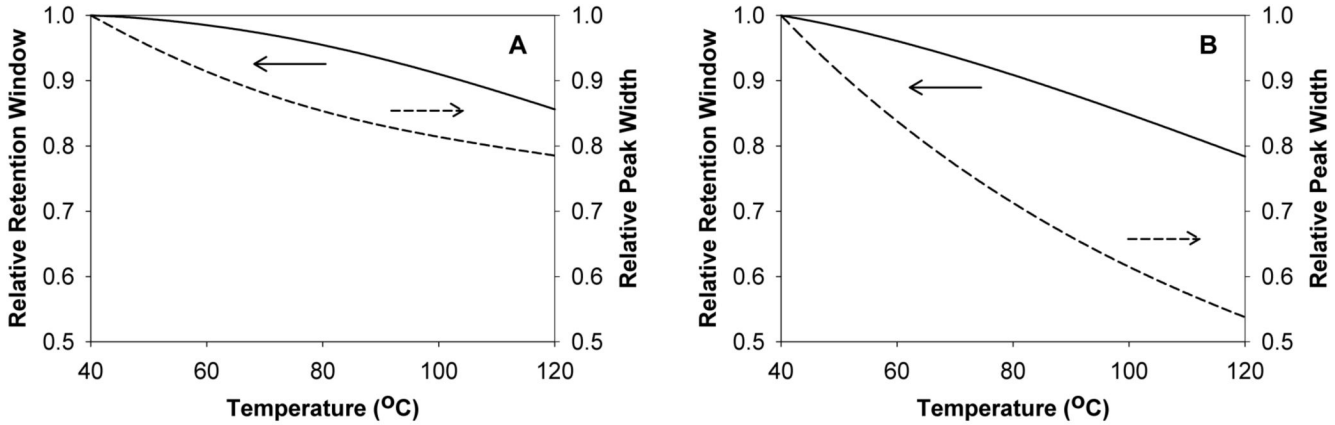

Figure 5.

Effect of temperature on relative retention window and average peak width at half height at (A) 0.50 mL/min and (B) 2.00 mL/min. The relative retention window and average peak width are normalized to their values at T = 40 °C. Other variables: same as Figure 2 except t_G = 30 min and ϕ_{final} = 0.43.

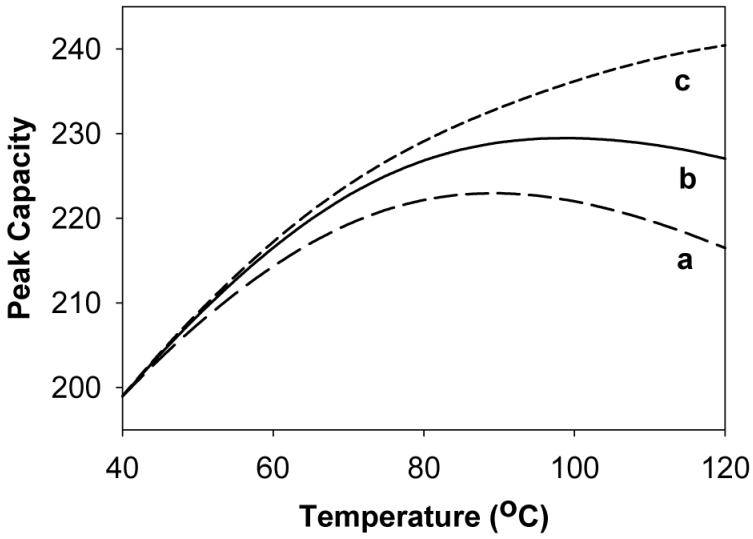

Figure 6.

Effect of temperature on peak capacity in three cases. Case a: ϕ_{final} is kept constant at 0.409 (--); Case b: ϕ_{final} is optimized by Solver to maximize peak capacity (—); Case c: Both ϕ_{final} and flow rate are simultaneously optimized by Solver to maximize peak capacity (----). Other variables at case 1: same as Figure 2 except F = 0.50 mL/min, t_G = 30 min and ϕ_{final} = 0.409.

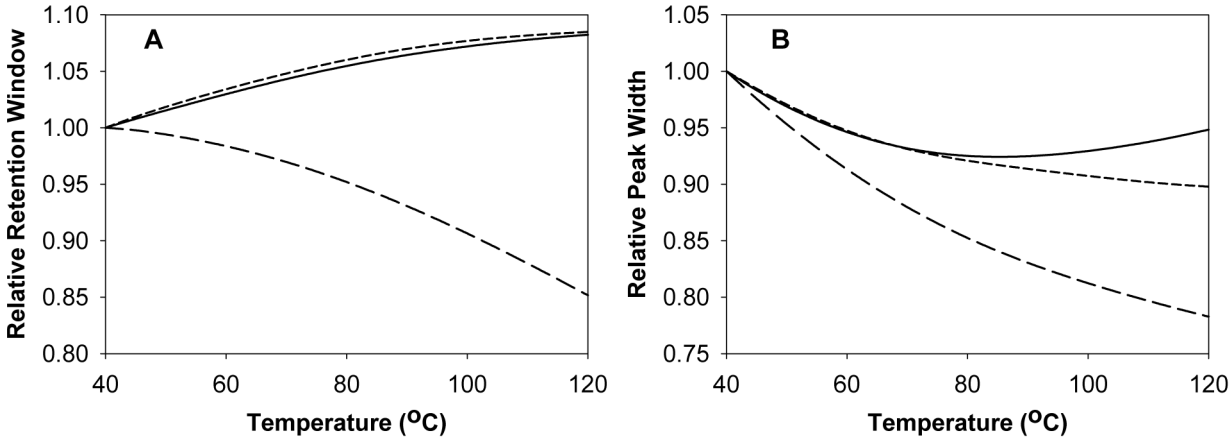

Figure 7.

Effect of temperature on (A) relative retention window and (B) relative average peak width at half height in the three cases described in Figure 7. The relative retention window and average peak width are normalized to their values at T = 40 °C.

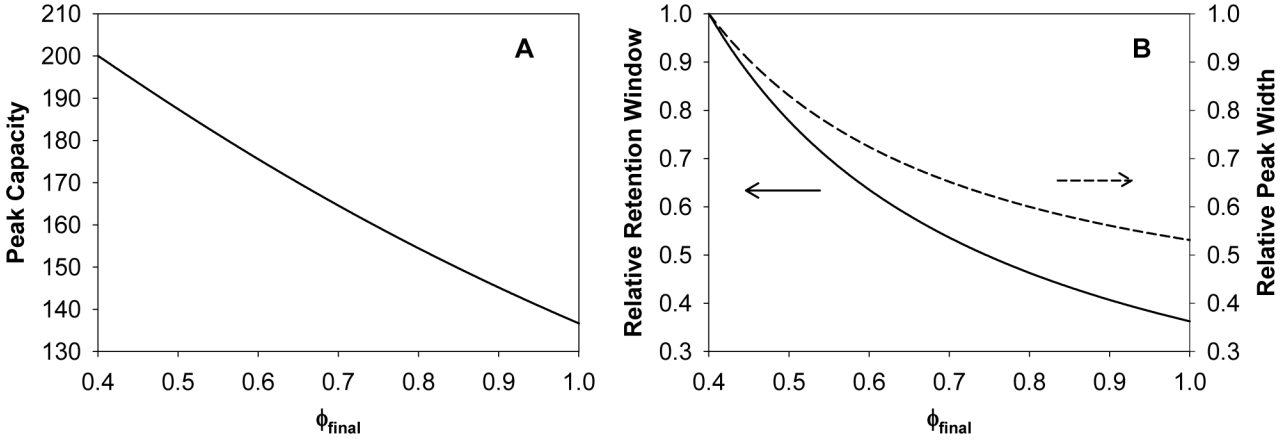

Figure 8.

Effect of ϕ_{final} on (A) peak capacity and (B) relative retention window and average peak width at half height. The relative retention window and average peak width are normalized to their values at ϕ_{final} of 0.40. Other variables: same as Figure 2 except F = 0.50 mL/min and t_G = 30 min.

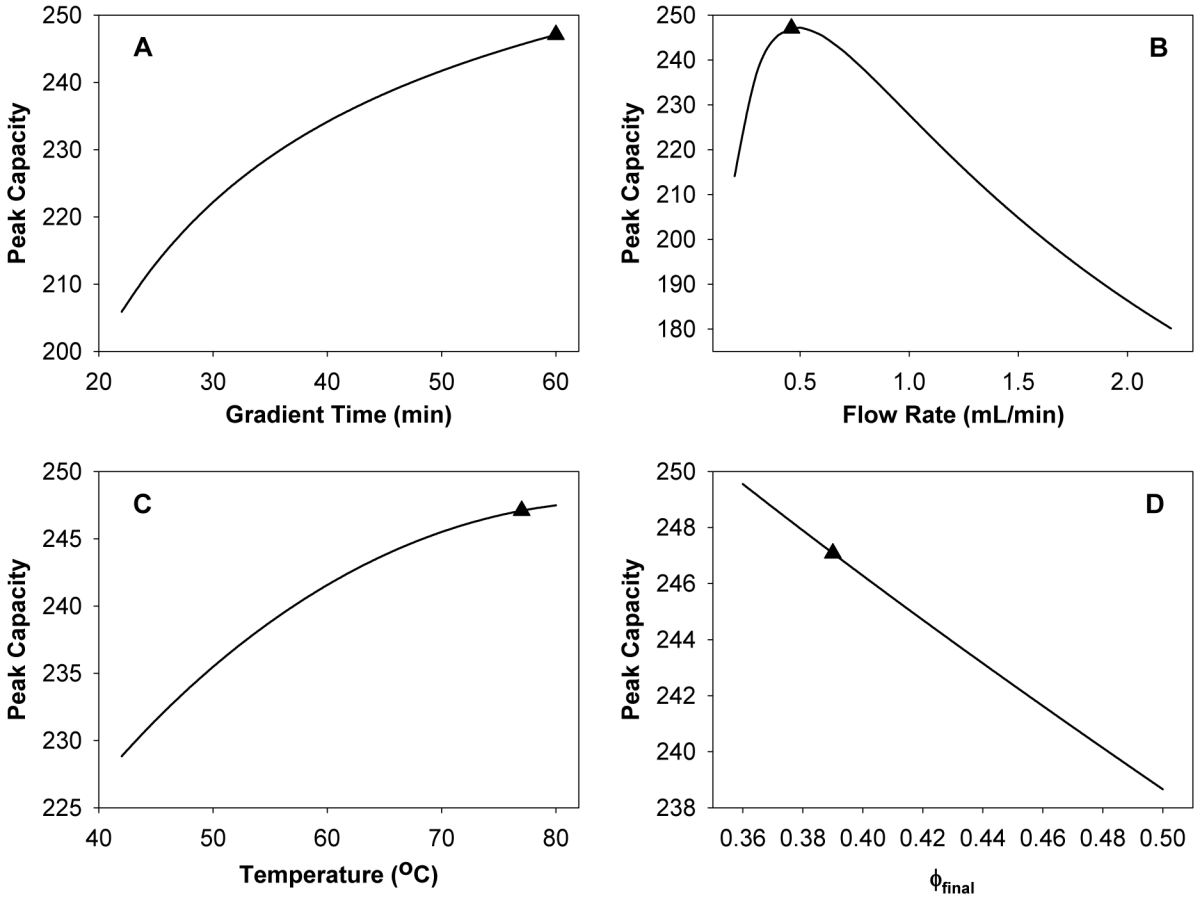

Figure 9.
Effect of (A) gradient time, (B) flow rate, (C) temperature, (D) ϕ_{final} on peak capacity for condition 1 in Table 3. Only one variable is changed while all other three variables are the same at those listed in condition 1. The original values in condition 1 are represented by solid triangle.

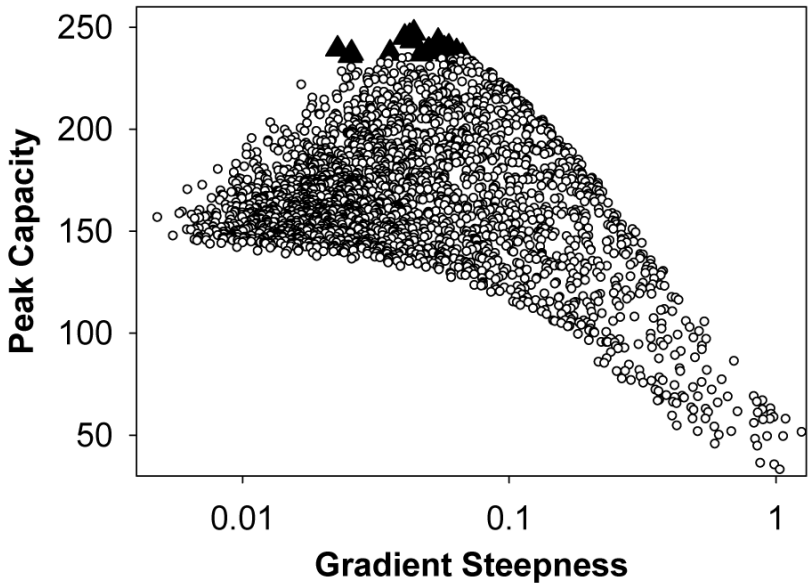

Figure 10.

Peak capacity vs. logarithmic gradient steepness in 2651 conditions generated in a Monte Carlo simulation. The best twenty conditions for peak capacity are represented by solid triangles; all other conditions are represented by open circles. Range of the variables in simulation: $0.10 < F < 3.80$ mL/min, $1 < t_G < 60$ min, $30 < T < 80$ °C, $0.30 < \phi_{final} < 0.60$.

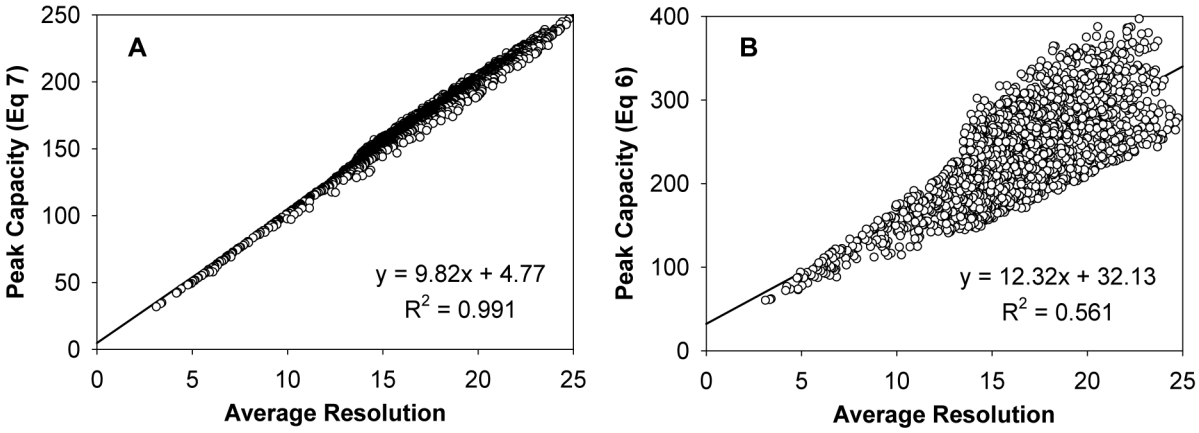

Figure 11.

Correlation of (A) peak capacity calculated via eq 7 and (B) peak capacity calculated via eq 6 with average resolution of eleven peptides. Each point represents one of the 2651 conditions generated in Monte Carlo simulation as in Figure 11. The linear regression lines are also displayed.

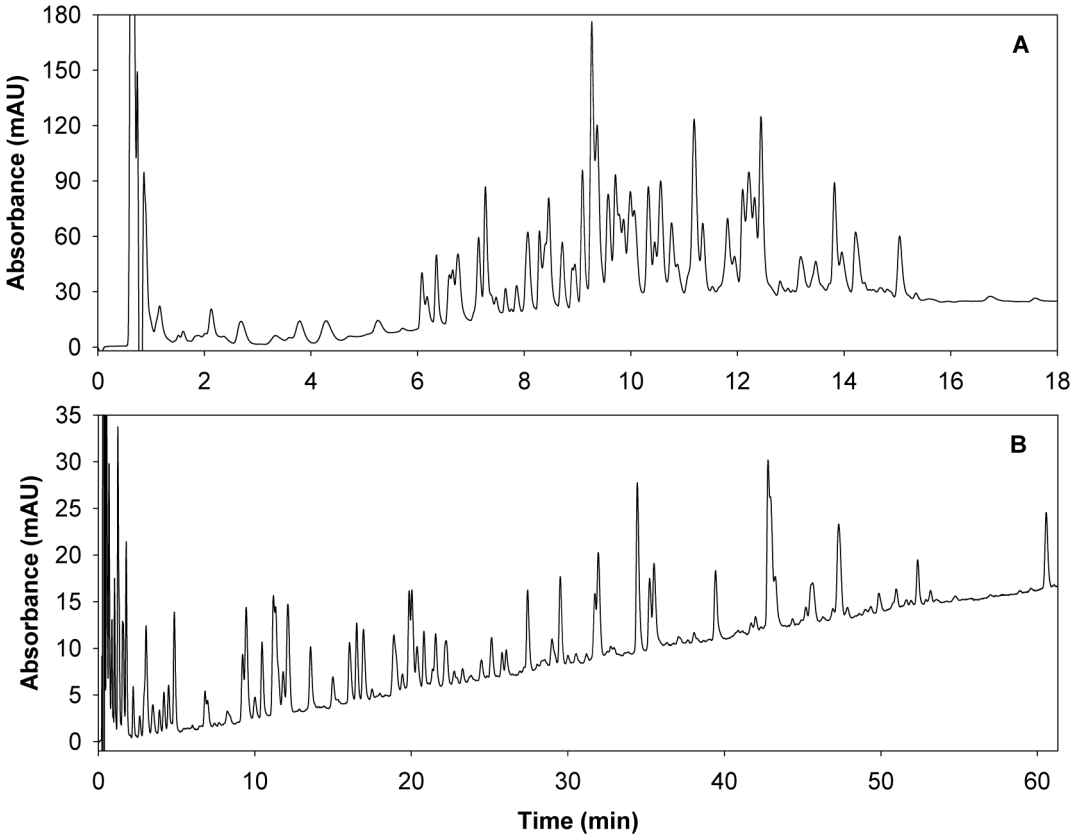

Figure 12.
Separation of BSA tryptic peptides under (A) Non-optimal conditions: 0.20 mL/min, room temperature, 5% to 59% ACN in 18 min and (B) Optimal conditions: 0.40 mL/min, 70 °C, 5% to 30% ACN in 60 min.

Table 1

Optimal Values of Flow Rate for Peak Capacity at Various ϕ_{final}[a]

	Optimized Values	
ϕ_{final}	F (mL/min)	nc**
0.40	0.51	247
0.45	0.53	244
0.50	0.54	240

[a] Flow rate was optimized using Solver. Conditions: t_G = 60 min, T = 80 °C, finitial = 0.05

Table 2

Optimal Values of Flow Rate and ϕ_{final} for Peak Capacity at Various Combinations of Gradient Time and Temperature[a]

		Optimized Values		
t_G (min)	T (°C)	F[b] (mL/min)	ϕ_{final}	n_c**
30	40	0.52	0.41	199
	80	0.62	0.37	229
	120[c]	0.86	0.31	240
60	40	0.35	0.40	230
	80	0.51	0.35	251
	120[c]	0.75	0.30	258
120	40	0.27	0.39	253
	80	0.45	0.34	267
	120[c]	0.72	0.28	272

[a] Flow rate and ffinal were simultaneously optimized using Solver with finitial = 0.05

[b] The minimum isocratic HETP at 40 °C on this column occurs at F = 0.40 mL/min based on a series of alkylphenone homologs

[c] The calculated results at 120 °C might not be as reliable as lower temperatures due to large extrapolation from experimental training runs

Table 3

Separation Conditions Providing the Five Best Peak Capacity Values from A Monte Carlo Simulation by Simultaneously Varying Flow Rate, Temperature, Gradient Time and ϕ_{final}[a]

Condition	F (mL/min)	T (°C)	ϕ_{final}	t_G(min)	b[b]	Δt_R(min)	$W_{1/2}$(min)	nc**[c]
1	0.46	77	0.39	60	0.044	53.34	0.127	247.1
2	0.47	69	0.38	59	0.042	55.01	0.132	245.5
3	0.53	76	0.40	58	0.041	49.99	0.120	245.1
4	0.52	74	0.41	57	0.043	48.19	0.117	243.4
5	0.39	69	0.40	59	0.054	52.52	0.127	243.0

[a] Range of the variables in simulation: $0.10 < F < 3.80$ mL/min, $1 < t_G < 60$ min, $30 < T < 80$ °C, $0.30 < \phi_{final} < 0.60$

[b] Gradient steepness calculated using an S value of 40

[c] Peak capacity calculated using equation 7